Thickness and production of sea ice in the Okhotsk Sea coastal polynyas from AMSR-E

Sohey Nihashi[1], Kay I. Ohshima[1], Takeshi Tamura[1], Yasushi Fukamachi[1], and Sei-ichi Saitoh[2]

S. Nihashi, Institute of Low Temperature Science, Hokkaido University, Sapporo 060-0819, Japan. (e-mail: sohey@lowtem.hokudai.ac.jp)

[1] Institute of Low Temperature Science, Hokkaido University, Sapporo, Japan

[2] Graduate School of Fisheries Sciences, Hokkaido University, Hakodate, Japan

Abstract. From comparisons with thickness of sea ice from AVHRR and ice-profiling sonar data, we have developed an AMSR-E thin ice thickness algorithm for the Sea of Okhotsk. This algorithm can estimate ice thickness of $\leq$0.2 m without snow using the polarization ratio of AMSR-E brightness temperature at 36.5 GHz channel from a linear relationship with AVHRR ice thickness. When a snow cover exists on the thin ice surface, as occurred a few times in each winter, it is shown that the algorithm cannot detect the thin ice. Sea-ice and dense shelf water (DSW) production in coastal polynya are estimated based on heat flux calculation with the daily AMSR-E ice thickness for 3 winters (December–March) of 2002/2003–2004/2005. The ice production is largest in the northwest shelf (NWS) polynya which accounts for $\sim$45% of the sum of ice production in major coastal polynyas. The ice production in major coastal polynyas would cover the maximum ice area of the Okhotsk Sea if the average ice thickness is assumed to be 1 m. Variability of the ice production is mainly modulated by air temperature. In the NWS polynya, which is the main DSW production area, the annual DSW formation rate is estimated to be $\sim$0.36 Sv.

1. Introduction

The Sea of Okhotsk is the southernmost sea with a sizeable seasonal ice cover in the Northern Hemisphere (Figure 1a). The initial freezing occurs at the northwest shelf region (Figure 1b) from late November. The sea-ice cover becomes maximum ($\sim$1.0$\times$10^6 km^2 on average) from the end of February to the beginning of March, when about 50–90% of the sea is covered with ice. Sea ice finally reaches the coast of Hokkaido around 44°N. The sea ice melts away by June. The major reason of the southernmost seasonal ice zone is that very cold air is blown over the sea from Siberia during autumn and winter by a prevailing northerly wind. At Verkhoyansk (67°33'N, 133°23'E) and Oymyakon (63°15'N, 143°9'E) in the Sakha Republic, Siberia, Russia, the lowest air temperature in the Northern Hemisphere has been recorded, and this region is called as the Pole of Cold. Also from the climatology of air temperature at 2 m (Figure 1a), this region is shown to be very cold (air temperature < -35°C).

In the northern part of the Sea of Okhotsk, coastal polynyas are formed by divergent ice drift due to prevailing offshore wind [*Martin et al.*, 1998]. Since the heat insulation effect of sea ice is greatly reduced in thin ice area, turbulent heat flux to the atmosphere at the coastal polynya surface is possibly two orders of magnitude larger than that at the surrounding thicker ice surface [*Maykut*, 1978]. Therefore, it has been considered that sea ice is formed very actively in the Okhotsk coastal polynyas, especially in the northwest shelf (NWS) region (Figure 1b) where the very cold air comes from the Pole of Cold due to the prevailing northerly wind (see Figure 6b later).

In the NWS polynya, dense shelf water (DSW) is formed due to large amount of brine rejection associated with the high ice production [*Shcherbina et al.*, 2003]. The DSW is the densest water as what is formed at the surface of both the Sea of Okhotsk and the North Pacific [*Kitani*, 1973], and is thought to be main source for ventilation of the North Pacific Intermediate Water (NPIW) [*Talley*, 1991; *Warner et al.*, 1996]. The DSW modified in the Sea of Okhotsk passes through the Kuril islands and spreads into the intermediate layer of the North Pacific [*Martin et al.*, 1998; *Shcherbina et al.*, 2003]. Thus, it can be said that, in the North Pacific, the Sea of Okhotsk is the only area where the surface water exposed to the atmosphere can be carried to the intermediate layer (at depths of 200–800 m) and that the DSW drives the overturning in the North Pacific. *Nakanowatari et al.* [2007] suggested that, during the past 50 years, warming and weakening of the overturning has occurred for the intermediate water in the northwestern North Pacific, originating from the Sea of Okhotsk. Therefore, to understand the climate system and the changes in the Sea of Okhotsk and the North Pacific regions, quantitative estimates of ice and DSW production in the Okhotsk coastal polynyas are considered to be very important.

Martin et al. [1998] detected both thin ice area and open water fraction by using brightness temperatures from Special Sensor Microwave Imager (SSM/I) with resolution of ∼25 km. Further, they estimated ice and DSW production in the Okhotsk coastal polynyas from heat flux calculation by assuming the ice thickness is uniformly 0.1 m. *Gladyshev et al.* [2000] estimated the DSW production by using similar methods as in *Martin et al.* [1998]. A sea-ice production map from heat flux calculation is shown in *Ohshima et al.* [2003], in which the sea-ice area was classified into 4 categories (open

water, new ice, young ice, and first-year ice) by using an ice type algorithm for SSM/I by *Kimura and Wakatsuchi* [1999] with a uniform ice thickness being assumed for each ice type. *Shcherbina et al.* [2004b] estimated DSW production in the NWS polynya from heat flux calculation by using ice types derived from SSM/I as in *Ohshima et al.* [2003]. Since heat loss to the atmosphere is fairly sensitive to ice thickness, especially when it is very thin, heat flux calculation using thin ice thickness based on observation is important to estimate ice and DSW production in the coastal polynya quantitatively. However, the polynya detection algorithm and the assumed ice thickness used in the previous studies were not validated by observational data. Further, because the spatial scale of coastal polynya is not large, use of spatially high-resolution data is also important.

From comparisons between brightness temperatures obtained from passive microwave radiometer onboard a ship and sea-ice data from in-situ measurements, *Hwang et al.* [2007] showed that the polarization ratio of the brightness temperature at 37 GHz vertically and horizontally polarized channels (in their study, $R_{37} = \frac{T_{B37V}}{T_{B37H}}$ was used following *Martin et al.* [2004]) is negatively correlated with thin ice thickness without snow. They also showed that this relationship is caused by the salinity of the ice surface, that is strongly correlated with the ice thickness. *Martin et al.* [2004] developed a thin ice thickness algorithm for SSM/I in the Chukchi Sea from comparison between the polarization ratio of the brightness temperature at 37 GHz channel (R_{37}) and ice thickness estimated by Advanced Very High Resolution Radiometer (AVHRR) infrared data [*Drucker et al.*, 2003]. Further, they estimated ice production in the coastal polynyas from heat flux calculation by using the SSM/I ice thickness. Their ice thickness algorithm was applied to brightness temperatures obtained from the Advanced Microwave Scanning Radiometer for EOS (AMSR-E) with

finer spatial resolution of ∼12.5 km [*Martin et al.*, 2005]. Also in the Antarctic Ocean, an ice thickness algorithm for SSM/I was developed [*Tamura et al.*, 2007], and ice production in coastal polynyas was estimated from heat flux calculation with the algorithm [*Tamura et al.*, 2008].

In this study, a thin ice thickness algorithm for AMSR-E is newly developed in the Sea of Okhotsk from comparisons with ice thicknesses from AVHRR infrared data. The accuracy of the AVHRR thickness is confirmed from comparisons with ice thicknesses from ice-profiling sonar which are more reliable. By using the daily AMSR-E ice thickness, ice production in coastal polynyas is estimated quantitatively from heat flux calculation. We also estimate DSW production from the obtained ice production. Further, we investigate variability of the Okhotsk coastal polynya and examine which meteorological parameter controls the ice and DSW production.

2. Data

In this study, the AMSR-E/Aqua L2A Global Swath Spatially-Resampled Brightness Temperatures [*Ashcroft and Wentz*, 2003] were used to estimate ice thickness and ice concentration. The number of satellite passes at a certain location per day is a function of latitude. AMSR-E can observe the Sea of Okhotsk (44°N–62°N) twice a day on an average. For the ice thickness algorithm, brightness temperatures at 36.5 GHz vertically and horizontally polarized channels that have lower sensitivity to water vapor were used. The mean spatial resolution of those channels is ∼12 km. The enhanced NASA Team (NT2) algorithm [*Markus and Cavalieri*, 2000] was used for the ice concentration calculation.

For the development of the AMSR-E ice thickness algorithm, we used ice thickness estimated from clear-sky infrared data from Advanced Very High Resolution Radiometer

(AVHRR) channels 4 and 5 on the National Oceanic and Atmospheric Administration (NOAA) -12 and -16 satellites (*e.g.* Figure 2a), received at the Faculty of Fisheries Sciences, Hokkaido University (Hakodate, Hokkaido, Japan). The spatial resolution is ∼1.1 km. In the image (Figure 2a), relatively smooth dark gray regions exist in the NWS region, coastal region of northeastern Sakhalin, and Terpenia Bay, surrounded by sea-ice cover shown by white or light gray. These dark gray regions correspond to coastal polynyas.

Ice draft measured by an ice-profiling sonar (IPS; ASL Environmental Sciences IPS4 420 kHz) in the coastal region of northeastern Sakhalin (52°43' N, 143°34' E; triangle in Figure 2a) was used to validate the AVHRR thickness. The IPS was moored from 27 December 2002 to 13 June 2003 at depths of ∼24 m. The sampling interval was 1 second. Values are typically accurate within ±0.05 m. The detail is described in *Fukamachi et al.* (in press).

For air temperatures at 2 m, dew point temperatures at 2 m, wind at 10 m, and surface sea level pressures (SLP), we used the twice daily (0000 UT and 1200 UT) data of European Centre for the Medium Range Weather Forecasts (ECMWF) with a spatial resolution of 2.5° × 2.5°. We also used geostrophic wind derived from the SLP. In this study, a relationship between the polynya area and wind is examined by using the geostrophic wind because ice advection is approximately parallel to the geostrophic wind [*Thorndike and Colony*, 1982]. The wind at 10 m is used for heat flux calculation. For cloud cover, we used the monthly averaged International Satellite Cloud Climatology Project (ISCCP) D2 data with resolution of 2.5° × 2.5°. For the heat flux calculations, these meteorological data were interpolated onto data points of AVHRR and AMSR-E L2A and polar

stereographic grid points with a Gaussian weighting function. The meteorological variables tend to have large gradients near the boundary between land and ocean. Thus, the weight function of the land points is reduced to be one-fifth for the interpolations of the air temperatures at 2 m, dew point temperatures at 2 m, and wind at 10 m following *Ohshima et al.* [2003]. The ECMWF wind speed was corrected by a factor of 1.25 and the ISCCP cloud cover is corrected by subtracting 0.08 following *Ohshima et al.* [2003]. We also used daily snow depth observed by a weather station at Ayan (Figure 1b).

3. AMSR-E Thin Ice Thickness Algorithm

In this study, a thin ice thickness algorithm is developed from a comparison between the polarization ratio of AMSR-E brightness temperature at 36.5 GHz vertically and horizontally polarized channels and ice thickness estimated using AVHRR infrared data. The method is similar to that of *Tamura et al.* [2007] conducted in the Antarctic using SSM/I data.

The AVHRR ice thickness is estimated following *Yu and Rothrock* [1996]. Their method is applicable to sea ice with thickness of <0.5 m. At first, ice surface temperature is calculated using AVHRR channel-4 and -5 data with the empirical equation proposed by *Key et al.* [1997]. Cases that are free from cloud and ice fog are manually chosen through a visual inspection of AVHRR channel-4 images. With this ice surface temperature, heat fluxes are calculated using the bulk and empirical formulae that are suitable for the Sea of Okhotsk [*Ohshima et al.*, 2003]. Ice bottom temperature is assumed to be the freezing point. For the heat flux calculation, 24-hour average of the twice daily ECMWF surface data is used as atmospheric input. The averaging is done by using the data closest to the time when the AVHRR data was acquired and the data at the previous time step (12

hours before). Ice thickness is estimated from conductive heat flux in ice by assuming that it balances with the heat flux between ice and atmosphere (*i.e.* heat budget at the ice surface is 0). To avoid the ambiguity caused by shortwave radiation absorption into the ice interior [*Grenfell and Maykut*, 1977], we choose AVHRR data obtained before sunrise. We assume that the heat flux between ice and atmosphere is a sum of net longwave radiation and turbulent heat flux. The similar ice thickness estimations using AVHRR data were made in the Beaufort Sea, Greenland Sea, Bering Sea, and off East Antarctica [*Yu and Rothrock*, 1996; *Drucker et al.*, 2003; *Tamura et al.*, 2006], and these studies showed that the method can estimate ice thickness within the error of ± 0.05 m from comparisons with in-situ observed ice thickness. Figure 2b shows the AVHRR ice thickness. In the regions which are expected to be coastal polynyas in Figure 2a, ice thickness increases monotonically from the coast.

Ice draft measured by the IPS in the coastal region of northeastern Sakhalin (triangle in Figure 2a) is used to validate the AVHRR ice thickness. For the comparison, the IPS ice draft is converted to ice thickness by assuming water density of 1026.7 kg m^{-3}, ice density of 920 kg m^{-3}, and no snow. The IPS ice thickness is averaged for 2 hours before and after acquisition of the AVHRR data ($\overline{h_I}$). The average of the AVHRR ice thickness of a pixel closest to the IPS site and the surrounding 8 pixels ($\overline{h_A}$) is used for the comparison. If we assume a typical ice drift of 0.5 m s^{-1}, migration scale with 2 hours becomes 3.6 km, which roughly corresponds to spatial scale of $\overline{h_A}$ (3 pixels). The 12 cases of ice thickness are estimated by using clear-sky AVHRR images. In Figure 3, the 10 cases are plotted because the other 2 cases exceed the maximum thickness of the method (0.5 m). Although the number of data is limited, $\overline{h_A}$ is correlated with $\overline{h_I}$ with a

correlation coefficient of 0.75 (Figure 3). The root mean square deviation is ∼0.01 m, and the regression line is represented by $\overline{h_A} = 1.10\overline{h_I} + 0.00$. These suggest that the method to estimate ice thickness from AVHRR infrared data is valid to some extent in the Sea of Okhotsk.

For comparing the AVHRR data with the AMSR-E data, the AVHRR ∼1.1 km gridded thermal ice thickness are mapped onto data points of AMSR-E L2A data. There are several tens of AVHRR pixels within a footprint of the AMSR-E data (∼14 km × 8 km). We use the hypothetical thermal ice thickness for which the calculated total heat flux from AVHRR data would be realized under the assumption of uniform ice thickness in the AMSR-E footprint, not the arithmetic average of the AVHRR thickness. This "thermal ice thickness" is suitable for heat loss calculation because the variability of surface fluxes is nonlinear with respect to that of ice thickness. Figure 4a shows the AVHRR thermal ice thickness (h_A) which is mapped onto data points of AMSR-E L2A.

Figure 4b shows spatial distribution of the polarization ratio of AMSR-E brightness temperature at 36.5 GHz channel ($PR_{36} = (T_{B36V} - T_{B36H})/(T_{B36V} + T_{B36H})$). The PR_{36} is transformed from R_{36} through the following equation: $PR_{36} = (R_{36} - 1)/(R_{36} + 1)$. The PR_{36} value is high at thin ice thickness (≤0.2 m) region. For the development of the AMSR-E ice thickness algorithm, the comparison between PR_{36} and the AVHRR thermal ice thickness is made for 3 boxes (northwest shelf region: NWS, coastal region of northeastern Sakhalin: SAK, and Terpenia Bay: TER) shown in Figure 4, based on clear-sky AVHRR infrared data of 35 cases obtained from 3 January to 18 March of 2003–2005. The numbers of the AVHRR data used in NWS, SAK, and TER are 17, 10, and 8, respectively. To see relationship clearly, the comparison is made at data points in

199 which the AVHRR ice thicknesses are nearly uniform within a footprint of AMSR-E L2A
200 data (≥80% of the AVHRR ice thicknesses are within ±0.05 m of the averaged value in
201 a footprint of AMSR-E L2A). With this criterion, the coastal polynya region is clearly
202 detected because the polynya region has relatively uniform ice thickness (Figure 2b).

203 Figure 5 is a scatterplot of PR_{36} versus h_A (hereafter PR_{36}–h_A plot) based on all of
204 the 35 clear-sky AVHRR infrared images. PR_{36} is negatively correlated with h_A. PR_{36}
205 is not sensitive to h_A when h_A is >0.3 m. An exponential relationship between PR_{36} and
206 the AVHRR thickness is shown in the Chukchi Sea [*Martin et al.,* 2004]. However, the
207 PR_{36}–h_A plot in the Sea of Okhotsk seems to be a nearly linear relationship for h_A <0.3
208 m. PR_{36}–h_A plots based on each AVHRR infrared image shows a more linear relationship
209 (not shown here). PR–h_A plots in the Antarctic Ocean based on the SSM/I brightness
210 temperatures at 37 GHz and 85GHz channels also show the similar linear relationship
211 [*Tamura et al.*, 2007]. In this study, an equation for thin ice thickness is obtained using
212 all data for thickness of ≤0.3 m in the 3 analysis areas. The slope of a line obtained
213 from least square fitting (dotted line in Figure 5) would be biased to a smaller value,
214 because h_A of <0 m does not exist and h_A of >0.3 m is not used while there are no
215 restrictions on the PR_{36} value. Particularly, the line does not represent the PR_{36}–h_A plot
216 around h_A of <0.05 m, which is a very important range for the algorithm and estimation
217 of ice production. Therefore, an equation for thin ice thickness is obtained based on a
218 principal component analysis which gives the line along which the projected data points
219 have maximum variance. The equation of the line is:

$$h_i = -3.78PR_{36} + 0.50, \quad (1)$$

where h_i is ice thickness in meters. The correlation coefficient between h_A and PR_{36} is -0.67. The root mean square deviation between the ice thicknesses from equation (1) and from AVHRR data, which is calculated in order to show error bars in Figure 5, is $\sim$0.05 m when h_i is $\leq$0.2 m, while it increases to 0.07–0.09 m when h_i is 0.2–0.3 m, because the PR_{36} value becomes insensitive to the ice thickness. In this study, ice thickness of $\leq$0.2 m is estimated from equation (1). The ice thickness is set to be 0.01 m when it is estimated to be $<$0.01 m. In the following, we treat ice area with thickness of $\leq$0.2 m as the coastal polynya. In the NWS region, *Ohshima et al.* [2003] showed that the surface heat loss over thin ice of 0.2 m is about 6 times larger than that over thick ice of 0.8 m with snow of 0.16 m (Table 1 in their study); this suggests that the heat loss in the thicker ice area is not so important.

Figure 2d shows daily mean thin ice thickness derived from AMSR-E using the equation (1). To reduce the effect of land contamination, if ice thickness at a grid point adjacent to land points is thicker than those at the surrounding grid points of the other side against the land point, it is substituted with the thinnest thickness among the surrounding grid points. Thin ice areas corresponding to coastal polynyas are clearly identified in the NWS, SAK, and TER regions. The areas and thicknesses correspond well with those of the AVHRR in the polynya areas (Figures 2b and 2d). At the ice edges, ice thickness is possibly underestimated due to contamination of an open water fraction whose brightness temperature is close to that of thin ice. In coastal polynyas, because sea ice is advected offshore simultaneously with freezing due to strong prevailing offshore wind, open water may exist in the area adjacent to the coast. However, ice surface temperatures estimated from the AVHRR infrared data having much finer resolution ($\sim$1.1 km) than AMSR-

E show that all pixels in the coastal polynyas are colder than the freezing point. This indicates that the open water area is very small and the coastal polynya is almost covered with thin ice under the spatial resolution of AMSR-E (∼12.5 km). We consider that the effect of the open water contamination on the thin ice algorithm is negligible for coastal polynyas. It is found from Figures 2c and 2d that the NT2 ice concentration algorithm tends to underestimate the concentration in the coastal polynya (new ice) regions, as shown in *Cavalieri et al.* [2006].

4. Ice Production and Dense Water Formation

In this section, ice and dense shelf water (DSW) production in the Okhotsk coastal polynyas is estimated from daily heat loss to the atmosphere (H). H is obtained from heat flux calculation using daily thin ice thickness derived from AMSR-E (*e.g.* Figure 2d). The procedure of the heat flux calculation is similar to that in the calculation of AVHRR ice thickness, except for inclusion of shortwave radiation. The analyses are made during 3 winters of 2002/2003–2004/2005.

Ice production rate per unit area (V_i) is estimated by assuming that all of H is used for sea-ice formation, and is given by

$$V_i = \frac{H}{\rho_i L_f}, \tag{2}$$

where ρ_i (= 920 kg m^{-3}) is the density of ice and L_f (= 0.234 MJ kg^{-1}) is the latent heat of fusion for ice. Oceanic heat flux due to the circulation and eddy mixing is assumed to be negligible. Water temperature is expected to be close to the freezing point over the entire water column because the coastal polynyas in the Sea of Okhotsk exist on the shallow

shelf ($\leq$200 m). Also data from the bottom moorings in the northwest shelf region, winter water temperature at the bottom layer was shown to be very close to the freezing point [*Shcherbina et al.*, 2003].

Figure 6a shows spatial distribution of cumulative ice production per unit area during winter (December–March), averaged from 2002/2003 to 2004/2005. The ice production is high in the NWS region, northern shelf (NS) region, and Gizhiga Bay (GIZ). The highest ice production (>10 m per winter) is shown in the narrow ($\sim$25 km) area along the coast of the NWS region.

Figure 6b shows air temperature at 2 m, sea level pressure (SLP), and geostrophic wind derived from the SLP, averaged over the 3 winters (December–March). The air temperature north of the NWS region, corresponding to the Pole of Cold, was shown to be < -36°C. In the NWS region, prevailing northerly-northeasterly wind with its speed of >20 m s^{-1} blows from this very cold region.

Table 1 summarizes the total heat loss and the cumulative ice production during the freezing period (December–March) in major coastal polynyas. The grouping of the analysis areas (Figure 1b) mostly follow *Martin et al.* [1998]. The ice production in the NWS polynya accounts for $\sim$45% of the total ice production in major coastal polynyas (TOTAL column in Table 1). The sum of the ice production in the NWS and NS polynyas reaches $\sim$65% of the total. Interannual variability of the total ice production in the major coastal polynyas is small during the 3 winters (Table 1).

From AMSR-E ice concentrations, the average of maximum ice area in the 3 winters is $\sim 1.0 \times 10^6$ km^2. If the ice thickness averaged over the sea-ice area in the Sea of Okhotsk is simply assumed to be 1 m, the maximum ice volume would be $\sim 10.0 \times 10^{11}$ m^3.

285 This ice volume is comparable to the total ice production in the major coastal polynyas
286 ($\sim 10.4 \times 10^{11}$ m^3 in Table 1).

287 Summary of monthly cumulative ice production averaged over the 3 winters (Table
288 2) shows that ice production in the NWS polynya is largest in December and gradually
289 decreases toward March. This is because ice thickness increases from the offshore, and
290 thus the polynya (thin ice) area becomes smaller (see Figure 7 later). The ice production
291 decreases considerably in March because of rapid increase of air temperature. Other
292 analysis areas also show similar decrease of ice production toward March although the
293 maximum is not always in December because the start of ice advance is different from
294 area to area.

295 Previous studies showed that the major dense shelf water (DSW) formation occurs in
296 the NWS polynya [*e.g. Gladyshev et al.*, 2000]. We also estimate the DSW production
297 in the NWS polynya, where the ice production was shown to be by far the largest (Table
298 1). Referring the observation by *Shcherbina et al.* [2004a], the constant water density
299 and salinity before (after) density enrichment are assumed to be $\rho_0 = 1026.25$kg m^{-3}
300 ($\rho_b = 1026.9$kg m^{-3}) and $s_0 = 32.6$ psu ($s_b = 33.4$ psu), respectively. Dense water volume
301 production rate per unit area (V_{DSW}) is obtained from salt flux due to brine rejection
302 (S_F) as follows:

$$V_{DSW} = \frac{S_F}{(\rho_b s_b - \rho_0 s_0)10^{-3}}. \tag{3}$$

303 S_F is given by

$$S_F = \rho_i V_i (s_0 - s_i)10^{-3}, \tag{4}$$

where s_i is the ice salinity and assumed to be constant ($s_i = 0.31 s_0$) following *Cavalieri and Martin* [1994]. V_i is given from equation (2). From ice production in the NWS polynya, the volume of DSW production averaged for the 3 winters is estimated to be $\sim 11.4 \times 10^{12}$ m^3. This corresponds to annual DSW formation rate of ∼0.36 Sv.

In the Sea of Okhotsk, the AMSR-E ice thickness algorithm of this study is the first one which is developed from a comparison with the AVHRR thickness validated by the IPS draft data. Further, because the spatial resolution of AMSR-E (∼12.5 km) is about two times finer than that of SSM/I (∼25 km) which has been used in previous studies, the AMSR-E thin ice thickness can better resolve the high ice production area close to the coast. Therefore, the ice and DSW production in the Okhotsk coastal polynyas estimated in this study is thought to be more reliable than that of previous studies, although comparison between the previous studies and this study should be done carefully because their analysis years are different. *Martin et al.* [1998] estimated the sum of the ice production for 65 days from 1 January in the NWS polynya to be $\sim 1.0 \times 10^{11}$ m^3 (Table 4 in their study), while it is $\sim 2.6 \times 10^{11}$ m^3 in this study. *Ohshima et al.* [2003] showed that maximum ice production is ∼5 m per winter from their ice production map (Figure 13 in their study), while it is ∼10 m per winter in this study (Figure 6a). We also estimated ice production for the same period of this study (2002/2003–2004/2005) using the similar method as in *Ohshima et al.* [2003] in which the ice type algorithm for SSM/I [*Kimura and Wakatsuchi*, 1999] is used. The ice production map showed that the maximum ice production in Figure 6a (∼10 m per winter) is reduced by half (not shown here). *Kimura and Wakatsuchi* [2004] estimated ice production in the NWS and NS regions to be 8.7×10^{11} m^2 from divergent ice motion derived from SSM/I. This areal ice

production corresponds to the ice production of 1.74 $\times 10^{11}$ m^3 with an ice thickness of 0.2 m. In this study, the ice production in these regions is 6.74 $\times 10^{11}$ m^3 (Table 1). Similarly, the annual DSW formation rate in the NWS polynya estimated from heat flux calculation in the previous studies are smaller than our estimation of 0.36 Sv. Values estimated by *Martin et al.* [1998], *Gladyshev et al.* [2000], and *Shcherbina et al.* [2004b] are 0.08–0.23 Sv, 0.13–0.34 Sv, and 0.27 Sv, respectively. *Shcherbina et al.* [2004b] also estimated the DSW formation rate to be 0.30 Sv based on the in-situ observation. The differences in the ice production and the DSW formation estimates are considered to be mainly caused by the difference in the spatial resolution between AMSR-E and SSM/I because ice thickness is thin (Figures 2b and 2d) and ice production is high (Figure 6a) near the coast. Similar difference in ice production due to the spatial resolution between AMSR-E and SSM/I is shown also in the Chukchi Sea polynyas [*Martin et al.*, 2005]. Further, the SSM/I (ice type) algorithm used in the previous studies was not validated by observations unlike our study. In the previous studies, the thin ice thickness is arbitrarily assumed. This tends to overestimate the thickness. Also, the difference in the algorithm is expected to be the other reason for the difference in the ice production and DSW formation estimates.

Finally, sensitivities of the heat loss (ice production) to errors in atmospheric input and in ice thickness estimation from AMSR-E are examined. *Ohshima et al.* [2003] estimated the sensitivities to errors in atmospheric input by assuming that the errors are the sum of bias and root mean square deviation between ECMWF/ISCCP data set and in-situ observed COADS data. In this study, we used the error values estimated by *Ohshima et al.* [2003] for our sensitivity analysis. Specifically, changing air temperature, dew point temperature, wind speed, and cloud factor by $\pm 1.2^{o}$C, $\pm 1.0^{o}$C, $\pm 14\%$, and $\pm 16\%$,

respectively, the heat loss (ice production) is re-estimated. Further, the sensitivity to errors in the AMSR-E ice thickness is also examined by changing the thickness by ± 0.05 m, based on root mean square deviation between the ice thickness from equation (1) and from AVHRR data (Figure 5). Table 3 summarizes the sensitivity analyses, showing that the heat loss (ice production) is the most sensitive to the error in ice thickness.

5. Intraseasonal variability of the NWS polynya

5.1. Relationships with meteorological parameters

In this section, we investigate the intraseasonal variability of the NWS polynya, where the ice production was shown to be by far largest, and examine which meteorological parameter mainly controls the heat loss to the atmosphere (ice and DSW production) in the polynya by showing the relationships among the heat loss and the meteorological parameters. Figure 7 shows daily time series of heat loss to the atmosphere integrated over thin ice (polynya) area (ice thickness $\leq$0.2 m), air temperature at 2 m, thin ice area, ice-covered area (ice concentration $\geq$15 %), increase in snow depth, and geostrophic wind in the NWS region during the 3 winters (December–March) of 2002/2003–2004/2005. The heat loss in the coastal polynya is negatively correlated with the air temperature, as expected (top panels). The analysis area in the NWS region is mostly covered by ice from January to March (second row of panels). From scatterplots from daily data for 2003–2005 winters (January–March), the heat loss in the coastal polynya is positively correlated with the thin ice (polynya) area with a high correlation coefficient of 0.91 (Figure 8a) and is negatively correlated with the air temperature which mainly controls sensible heat flux with a correlation coefficient of -0.76 (Figure 8b). On the other hand, wind speed at

370 10 m, which is one of the important factors controlling the turbulent heat flux, does not
371 show clear relationship with the heat loss (Figure 8c).

372 The prevailing winds or oceanic currents that cause divergent ice motion is the main
373 cause for enlargement of coastal polynya. In the NWS region, *Martin et al.* [1998] showed
374 that interannual variability of the polynya area is determined by the offshore component
375 of the wind. Daily time series of geostrophic wind vector shows that northerly wind is
376 dominant during winter in the NWS region (bottom panels in Figure 7). The thin ice
377 (polynya) area tends to be large when offshore component of the geostrophic wind is
378 large (second row of panels from the top in Figure 7). A scatterplot shows that offshore
379 component of the geostrophic wind is positively correlated with the thin ice (polynya)
380 area with a correlation coefficient of 0.54 (Figure 9a). Since heat loss to the atmosphere
381 in coastal polynya depends on the polynya area (Figure 8a), the offshore component of
382 the geostrophic wind is also positively correlated with the heat loss with a correlation
383 coefficient of 0.51 (Figure 9b). These comparisons with the offshore wind (Figure 9) were
384 made by advancing the wind data by 1 day because a correlation coefficient is highest at
385 1-day lag from a lag correlation analysis (not shown here).

386 The results of this study indicate that the heat loss to the atmosphere in coastal polynya
387 is mainly modulated by the air temperature at 2 m and the offshore component of the
388 geostrophic wind (Figures 8b and 9b). We carry out a multiple linear regression anal-
389 ysis using daily data for the 3 winters (January–March) to show which meteorological
390 parameter contributes more to the heat loss. In the analysis, the heat loss is treated as
391 dependent variable, and the air temperature and the offshore wind as explanation vari-
392 ables. The multiple regression explains 62% of the variance. The standardized partial

393 regression coefficients of the air temperature and the wind are −0.65 and 0.25, respec-
394 tively. These coefficients are significant at 99.5%. The results indicate that variability of
395 heat loss is best correlated with that of the air temperature.

5.2. Rapid reduction of polynya area, and its relationship with snow cover

396 For the 3 winters, the polynya area occasionally reduced rapidly (second row of panels
397 from the top in Figure 7). In the following, we examine the causes of the rapid polynya
398 closure in the case of 20–21 January 2003 as an example. Left panels in Figure 10 show
399 timeseries of AMSR-E ice thickness map in the NWS region from 20 to 21 January 2003.
400 The map at 17:02 UT on 20 January shows that the ice thickness east of the coastal
401 polynya became thick (ice thickness >0.2 m), when compared to the map at 3:01 UT of
402 that day. Only ∼9 hours later (2:05 UT on 21 January), the thick ice region advanced
403 by >100 km to the west, and the polynya area almost disappeared, except for the region
404 very close to the coast. Right panels in Figure 10 show timeseries of daily sea level
405 pressure, geostrophic wind, and air temperature at 2 m from 19 to 21 January 2003. A
406 low pressure system east of the Kamchatka Peninsula moved into the Sea of Okhotsk
407 during this period. Subsequently, the wind in the northern part of the Sea of Okhotsk
408 was changed from northerly to easterly from the eastern side. Relatively warm air was
409 advected from the Pacific Ocean due to this wind direction change.

410 The polynya area retreated by >100 km in ∼9 hours (left panels in Figure 10). If the ice
411 drift speed is assumed to be 2% of the geostrophic wind [*Kimura and Wakatsuchi*, 1999],
412 sea ice is advected by only ∼13 km by the wind drift because the wind speed is at most
413 20 m s^{-1}. This indicates that the rapid polynya closure cannot be explained only from
414 the wind drift of the offshore thick ice. Thin ice which covers the coastal polynya (*e.g.*

nilas or pancake ice) can be piled up easily. It was shown that the process of piling up of thin ice is important for ice growth in the southern part of the Sea of Okhotsk [*Toyota et al.*, 2004; *Fukamachi et al.*, 2006]. However, this effect is also thought to be not enough to explain the rapid polynya closure because of the small ice advection by wind.

From the heat budget analysis with meteorological conditions averaged over this period in the NWS region, it is shown that thin ice whose thickness is ∼0.05 m grows locally by ∼0.08 m day^{-1}, and thus the ice thickness cannot exceed 0.2 m within 9 hours. Therefore, the rapid polynya closure cannot be explained by the local thermal balance solely.

Third row of panels from the top in Figure 7 show daily increase in snow depth at Ayan (Figures 1b and 10) adjacent to the NWS polynya. The snow depth increased by ∼0.15 m for 4 days from 21 January 2003. This is the maximum increase in the snow depth during winter of the 2002/2003 season. In the NWS polynya region, since northerly wind from the continent is dominant, the advected air is very cold and dry. However, during the period of this rapid polynya closure, snowfall may have been brought to the polynya area by relatively warm and humid air that was advected from the open ocean (the Pacific Ocean) due to the change in wind directions associated with the moving low pressure system. If this is the case, information through microwave from the thin ice surface would be hidden by the snow cover and the AMSR-E ice thickness algorithm would estimate the ice as thicker ice (>0.2 m) because the PR_{36} is shifted to the lower value [*Hwang et al.*, 2007]. We conclude that the apparent rapid polynya closure is an artifact of the AMSR-E algorithm not being able to detect thin ice under the snow cover.

Other rapid polynya area reductions occurred on 6 February 2003, 21 January 2004, 10 March 2004, 26 March 2004, 8 January 2005, 27 January 2005, and 22 March 2005

(second row of panels from the top in Figure 7). Most of these cases show that the ice thickness increased rapidly from offshore as in the case of 20–21 January 2003 (left panels in Figure 10) and that the snow depth at Ayan increased (third row of panels from the top in Figure 7). We consider that these reductions are also apparent ones owing to that the AMSR-E algorithm cannot detect thin ice due to a snow cover on ice.

6. Summary and Discussion

A thin ice thickness algorithm for AMSR-E was newly developed in the Sea of Okhotsk base on a comparison between the polarization ratio of AMSR-E brightness temperature at 36.5 GHz vertically and horizontally polarized channels (PR_{36}), and ice thickness estimated using AVHRR infrared data (Figure 5). The AVHRR thickness was validated by comparison with ice thickness measured by an ice-profiling sonar in the coastal region of northeastern Sakhalin (Figure 3). The algorithm can estimate ice thickness of $\leq$0.2 m without a snow cover from a linear relationship between the PR_{36} and the AVHRR thickness (equation 1).

We estimated ice production in major Okhotsk coastal polynyas during 3 winters of 2002/2003–2004/2005 (Table 1) from heat flux calculation in which the daily AMSR-E ice thickness (*e.g.* Figure 2d) is used. Oceanic heat flux due to the circulation and eddy mixing was assumed to be negligible. Interannual variability of the ice production was small among the 3 winters. The sum of the ice production during winter in the Okhotsk coastal polynyas would cover the maximum ice area if the average ice thickness is assumed to be 1 m. The ice production was highest in the northwest shelf (NWS) region (Table 1 and Figure 6a) as in the previous studies [*Martin et al.*, 1998; *Ohshima et al.*, 2003]. Our estimation shows that $\sim$45% of the total ice production in the Okhotsk polynyas

is attributable to the NWS polynya (Table 1). In the NWS region, the cumulative ice production during winter (December–March) was especially high (>10 m per winter) within ∼25 km from the coast (Figure 6a). The NWS region corresponds to the area where very cold air is advected from the Pole of Cold, Siberia, by prevailing northerly wind (Figure 6b). The annual dense shelf water formation rate in the NWS polynya was estimated to be ∼0.36 Sv.

The size of the NWS polynya is comparable to that of the Ross Sea polynya which is the largest coastal polynya with the highest ice production in the Antarctic Ocean. From the comparison with ice production in the Ross Sea polynya estimated by the similar method (Figure 1 in *Tamura et al.* [2008]), the maximum value of annual cumulative ice production in the NWS polynya (Figure 6a) is ∼65% of that in the Ross Sea polynya (∼16 m per winter). This suggests that ice production per unit time in the NWS polynya is comparable to that in the Ross Sea polynya, considering that the winter period of the Okhotsk Sea is about half of the Antarctic. In the NWS polynya, the densest water at the surface of both the Sea of Okhotsk and the North Pacific is considered to be formed.

We examined relationships between heat loss to the atmosphere and meteorological parameters that are considered to mainly control the heat loss in the NWS polynya. The heat loss is negatively correlated with air temperature at 2 m with a correlation coefficient of −0.76 (Figure 8b) and is positively correlated with the offshore component of the geostrophic wind, which controls the polynya area, with a correlation coefficient of 0.51 (Figure 9b). From a multiple linear regression analysis, it was shown that the heat loss in the coastal polynya is mainly governed by the air temperature (the standardized

partial regression coefficients of the air temperature and the offshore wind are −0.65 and 0.25, respectively).

The rapid polynya closures that cannot be explained both dynamically and thermodynamically were observed (Figures 7 and 10). These rapid closures coincide with snowfall suggesting that our AMSR-E algorithm cannot detect thin ice if a snow cover exists on ice. This is because information through microwave from the thin ice surface would be masked by the snow cover that has the lower value of PR_{36}, similar value to that of thick ice. The snow can mask the ice even if it is quite thin (<0.02 m; *Hwang et al.* [2007]). However, the effect of snow does not affect heat loss (ice production) estimation because of the heat insulation effect of snow (thermal conductivity of snow is about one-seventh of ice). For example, if snow of 0.02 m (0.1 m) depth exists on ice of 0.1 m thickness, the insulation effect corresponds to ice of ∼0.24 m (∼0.8 m) without snow. Thus, it can be considered that the cumulative ice production map (Figure 6a) is still valid even if the AMSR-E algorithm cannot detect thin ice with snow cover.

The AMSR-E data used in this study are quite useful to examine relatively small spatial scale phenomena because of the finer resolution than the SSM/I data. However, the accumulation of the AMSR-E data is still insufficient to discuss long-term variation because the data are available only from June 2002. On the other hand, the SSM/I data, whose resolution is relatively coarse, is available from July 1987 and has been accumulated more than 20 years. By developing a SSM/I thin ice thickness algorithm, and from a comparison of the AMSR-E and SSM/I data during the overlapping period, interannual variability of ice production could be examined.

Acknowledgments. The AMSR-E data were provided by the National Snow and Ice Data Center (NSIDC), University of Colorado. The snow depth data at Ayan were provided by the National Climatic Data Center (NCDC). Discussion with Takenobu Toyota was very helpful. This work was supported by RR2002 of the Project for Sustainable Coexistence of Human, Nature, and the Earth within the Japanese Ministry of Education, Culture, Sports, Science and Technology (MEXT), and by Grant-in-Aids for Scientific Research (21740337, 20221001, and 17540405) of the MEXT. This work was also supported by research fund for Global Change Observation Mission 1st - Water (GCOM-W1) of the Japan Aerospace Exploration Agency (JAXA).

References

Ashcroft, P., and F. Wentz (2003), updated daily, AMSR-E/Aqua L2A global swath spatially-resampled brightness temperatures (Tb) V002, National Snow and Ice Data Center, Boulder, Colorado, Digital media.

Cavalieri, D. J., T. Markus, D. K. Hall, A. J. Gasiewski, M. Klein, and A. Ivanoff (2006), Assessment of EOS Aqua AMSR-E Arctic sea ice concentrations using Landsat-7 and airborne microwave imagery, *IEEE Trans. Geosci. Remote Sens.*, *44*, 3057–3069.

Cavalieri, D. J., and S. Martin (1994), The contribution of Alaskan, Siberian, and Canadian coastal polynyas to the cold halocline layer of the Arctic Ocean, *J. Geophys. Res.*, *99*, 18,343–18,362.

Cavalieri, D. J., C. Parkinson, P. Gloersen, and H. J. Zwally (1996), updated 2006, Sea ice concentrations from Nimbus-7 SMMR and DMSP SSM/I passive microwave data, February 1979–2002, National Snow and Ice Data Center, Boulder, Colorado, Digital

525 media.

526 Drucker, R., S. Martin, and R. Moritz (2003), Observations of ice thickness and frazil ice
527 in the St. Lawrence Island polynya from satellite imagery, upward looking sonar, and
528 salinity/temperature moorings, *J. Geophys. Res.*, *108*, 3149, doi:10.1029/2001JC001213.

529 Fukamachi, Y., G. Mizuta, K. I. Ohshima, T. Toyota, N. Kimura, and M. Wakatsuchi
530 (2006), Sea ice thickness in the southwestern Sea of Okhotsk revealed by a moored
531 ice-profiling sonar, *J. Geophys. Res.*, *111*, C09018, doi:10.1029/2005JC003327.

532 Fukamachi, Y., K. Shirasawa, A. M. Polomoshnov, K. I. Ohshima, E. Kalinin, S. Nihashi,
533 H. Melling, G. Mizuta, and M. Wakatsuchi, Direct observations of sea-ice thickness and
534 brine rejection off Sakhalin in the Sea of Okhotsk, *Continental Shelf Research*, in press.

535 Gladyshev, S., S. Martin, S. Riser, and A. Figukin (2000), Dense water production on the
536 northern Okhotsk shelves: Comparison of ship-based spring–summer observations for
537 1996 and 1997 with satellite observations, *J. Geophys. Res.*, *105*, 26,281–26,299.

538 Grenfell, T. C., and G. A. Maykut (1977), The optical properties of ice and snow in the
539 Arctic Basin., *J. Glaciol.*, *18*, 445–463.

540 Hwang, B. J., J. K. Ehn, D. G. Barber, R. Galley, and T. C. Grenfell (2007), Investigations
541 of newly formed sea ice in the Cape Bathurst polynya: 2. Microwave emission, *J.*
542 *Geophys. Res.*, *112*, C05003, doi:10.1029/2006JC003703.

543 Key, J., J. Collins, C. Fowler, and R. Stone (1997), High-latitude surface temperature
544 estimates from thermal satellite data, *Remote Sens. Environ.*, *61*, 302–309.

545 Kimura, N., and M. Wakatsuchi (1999), Processes controlling the advance and retreat of
546 sea ice in the Sea of Okhotsk, *J. Geophys. Res.*, *104*, 11,137–11,150.

547 Kimura, N. and M. Wakatsuchi (2004), Increase and decrease of sea ice area in the Sea of
548 Okhotsk: ice production in coastal polynyas and dynamical thickening in convergence
549 zones, *J. Geophys. Res.*, *109*, C09S03, doi: 10.1029/2003JC001901.

550 Kitani, K. (1973), An oceanographic study of the Okhotsk Sea — Particularly in regard
551 to cold waters, *Bull. Far Seas Fish Res. Lab.*, *9*, 45–76.

552 Markus, T., and D. J. Cavalieri (2000), An enhancement of the NASA Team sea ice
553 algorithm, *IEEE Trans. Geosci. Remote Sens.*, *38*, 1387–1398.

554 Martin, S., R. Drucker, and K. Yamashita (1998), The production of ice and dense shelf
555 water in the Okhotsk Sea polynyas, *J. Geophys. Res.*, *103*, 27,771–27,782.

556 Martin, S., R. Drucker, R. Kwok, and B. Holt (2004), Estimation of the thin ice
557 thickness and heat flux for the Chukchi Sea Alaskan coast polynya from Spe-
558 cial Sensor Microwave/Imager data, 1990-2001, *J. Geophys. Res.*, *109*, C10012,
559 doi:10.1029/2004JC002428.

560 Martin, S., R. Drucker, R. Kwok, and B. Holt (2005), Improvements in the estimates
561 of ice thickness and production in the Chukchi Sea polynyas derived from AMSR-E,
562 *Geophys. Res. Lett.*, *32*, L05505, doi:10.1029/2004GL022013.

563 Maykut, G. A. (1978), Energy exchange over young sea ice in the central Arctic, *J.*
564 *Geophys. Res.*, *83*, 3646–3658.

565 Nakanowatari, T., K. I. Ohshima, and M. Wakatsuchi (2007), Warming and oxy-
566 gen decrease of intermediate water in the northwestern North Pacific, originat-
567 ing from the Sea of Okhotsk, 1995–2004,*Geophysical Research Letters*, *34*, L04602,
568 doi:10.1029/2006GL028243.

569 Ohshima, K. I., T. Watanabe, and S. Nihashi (2003), Surface heat budget of the Sea
570 of Okhotsk during 1987–2001 and the role of sea ice on it, *J. Meteorol. Soc. Jpn.*, *81*,
571 653–677.

572 Shcherbina, A. Y., L. D. Talley, and D. L. Rudnick (2003), Direct observations of North
573 Pacific Ventilation: Brine rejection in the Okhotsk Sea, *Science*, *302*, 1952–1955.

574 Shcherbina, A. Y., L. D. Talley, and D. L. Rudnick (2004a), Dense water formation on
575 the northwestern shelf of the Okhotsk Sea: 1. Direct observations of brine rejection, *J.*
576 *Geophys. Res.*, *109*, C09S08, doi:10.1029/2003JC002196.

577 Shcherbina, A. Y., L. D. Talley, and D. L. Rudnick (2004b), Dense water formation on
578 the northwestern shelf of the Okhotsk Sea: 2. Quantifying the transports, *J. Geophys.*
579 *Res.*, *109*, C09S09, doi:10.1029/2003JC002197.

580 Talley, L. D. (1991), An Okhotsk water anomaly: Implications for ventilation in the North
581 Pacific, *Deep Sea Res.*, *38*, Suppl. 1, S171–S190.

582 Tamura, T., K. I. Ohshima, H. Enomoto, K. Tateyama, A. Muto, S. Ushio, and R. A.
583 Massom (2006), Estimation of thin sea-ice thickness from NOAA AVHRR data in a
584 polynya of the Wilkes Land coast, East Antarctica, *Ann. Glaciol.*, *44*, 269–274.

585 Tamura, T., K. I. Ohshima, T. Markus, D. J. Cavalieri, S. Nihashi, and N. Hirasawa
586 (2007), Estimation of thin ice thickness and detection of fast ice from SSM/I data in
587 the Antarctic Ocean, *J. Atmos. Ocean. Tech.*, *24*, 1757–1772.

588 Tamura, T., K. I. Ohshima, and S. Nihashi (2008), Mapping of sea ice production for
589 Antarctic coastal polynyas, *Geophys. Res. Lett.*, *35*, doi:10.1029/2007GL032903.

590 Thorndike, A. S., and R. Colony (1982), Sea ice motion in response to geostrophic winds,
591 *J. Geophys. Res.*, *87*, 5845–5852.

592 Toyota, T., T. Kawamura, K. I. Ohshima, H. Shimoda, and M. Wakatsuchi (2004), Thick-
593 ness distribution, texture and stratigraphy, and a simple probabilistic model for dynam-
594 ical thickening of sea ice in the southern Sea of Okhotsk. *J. Geophys. Res.*, *109*, C06001,
595 doi:10.1029/2003JC002090.
596 Warner, M. J., J. L. Bullister, D. P. Wisegarver, and R. H. Gammon (1996), Basin-wide
597 distributions of chlorofluorocarbons CFC-11 and CFC-12 in the North Pacific: 1985–
598 1989, *J. Geophys. Res.*, *101*, 20,525–20542.
599 Yu, Y., and D. A. Rothrock (1996), Thin ice thickness from satellite thermal imagery, *J.*
600 *Geophys. Res.*, *101*, 25,753–25,766.

Figure 1. (a) Map of sea ice and air temperature at 2 m in February averaged from 1979 to 2002. White regions indicate the sea-ice area (ice concentration $\geq$15%). Ice concentrations from Nimbus-7 SMMR and DMSP SSM/I [*Cavalieri et al.*, 1996, updated 2006] are used. Black (white) contours indicate the air temperature below (above) 0°C. Air temperature is from the European Centre for the Medium-Range Weather Forecasts Re-Analysis (ERA-40) data set. The rectangle corresponds to the map shown in (b). (b) Map of the Sea of Okhotsk with bottom topography. The 200- and 3000-m isobars are indicated by thin lines. Thick lines indicate the analysis area in the northwest shelf region (NWS), north shelf region (NS), Gizhiga Bay (GIZ), coastal regions of western Kamchatka (KAM) and northeastern Sakhalin (SAK), and Terpenia Bay (TER), respectively. The crosses and circles indicate the grid points of ECMWF data used in Figures 7, 8, and 9.

Figure 2. Maps of sea ice on 8 March 2003. (a) Infrared image of AVHRR ch. 4. The location of the ice-profiling sonar observation is shown by a red triangle. (b) Ice thickness derived from AVHRR infrared data. (c) Ice concentration derived from AMSR-E. (d) Thin ice thickness derived from AMSR-E. The Japan Sea and the open ocean regions (ice conc. <15%) are masked by black.

Figure 3. Comparison between ice thicknesses from the ice-profiling sonar and AVHRR infrared data. Error bars indicate uncertainty of the thickness (both of them are 0.05 m). The details are described in the text.

Figure 4. (a) Thermal ice thickness derived from AVHRR infrared data and (b) the polarization ratio of AMSR-E brightness temperature at 36.5 GHz vertically and horizontally polarized channels (PR_{36}) on 8 March 2003. Data are mapped onto data points of the AMSR-E L2A. The open ocean region (ice conc. <15%) is masked by black.

Figure 5. Scatterplot of the polarization ratio of AMSR-E brightness temperature at 36.5 GHz channel (PR_{36}) versus AVHRR thermal ice thickness. AVHRR infrared data of 35 cloud- and fog-free cases are used. The data are obtained from the 3 polynya regions indicated by rectangles in Figure 4. The solid line indicates the principal component axis represented by equation (1). The dotted line indicates the line obtained from least square fitting. The vertical lines with crossbars show the root mean square deviation between the ice thicknesses from equation (1) and from AVHRR data. The details are described in the text.

Figure 6. (a) Spatial distribution of cumulative sea-ice production during winter (December–March) averaged from 2002/2003 to 2004/2005 seasons. Gray lines denote mean February ice extent averaged from 2003 to 2005. The Japan Sea is masked by black. (b) Sea level pressure (solid lines), geostrophic wind (vectors), and air temperature at 2m (shades), averaged during winter (December–March) of 2002/2003–2004/2005.

Figure 7. Daily timeseries of polynya characteristics and meteorological conditions in the NWS region (Figure 1b) from 2002/2003 to 2004/2005 seasons. Top panels show heat loss to the atmosphere in thin ice ($\leq$0.2 m) area (solid line) and air temperature at 2 m averaged over 3 locations, marked by the circles in Figure 1b (dotted line). The second row of panels from the top show the thin ice area (solid line) and offshore component of geostrophic wind averaged over 12 location, marked by the crosses in Figure 1b (dotted line). Shade indicates ice area (ice conc. $\geq$15%). Dashed horizontal line indicates the area of the NWS region. The third row of panels show increase in snow depth at Ayan (Figure 1b). Bottom panels show geostrophic wind vector averaged over 12 locations, marked by the crosses in Figure 1b. Horizontal and vertical axes correspond to alongshore and offshore directions, respectively.

Figure 8. Scatterplots of (a) thin ice ($\leq$0.2 m) area, (b) air temperature at 2 m, and (c) wind speed at 10 m versus heat loss to the atmosphere in the NWS region. Daily data obtained from 1 January to 31 March during 2003–2005 are used. The temperature and the wind speed averaged over 3 locations, marked by the circles in Figure 1b are used.

Figure 9. Scatterplots of the offshore component of geostrophic wind versus (a) thin ice ($\leq$0.2 m) area and (b) heat loss to the atmosphere in the NWS region. Daily data obtained from 1 January to 31 March during 2003–2005 are used. The offshore wind speed is advanced by 1 day. The wind speed averaged over 12 locations, marked by the crosses in Figure 1b is used.

Figure 10. Twice daily maps of spatial distribution of thin ice thickness from 20 to 21 January 2003 (left panels). Daily (1200 UT) maps of sea level pressure (solid lines), geostrophic wind (vectors), and air temperature at 2 m (shades) from 19 to 21 January 2003 (right panels). The rectangle in the right panels indicates the area of the thin ice thickness map (left panels).

Table 1. Summary of heat loss to the atmosphere and cumulative ice production in coastal polynyas during winter (December–March) of 2002/2003–2004/2005 in the northwest shelf region (NWS), north shelf region (NS), Gizhiga Bay (GIZ), coastal regions of western Kamchatka (KAM) and northeastern Sakhalin (SAK), and Terpenia Bay (TER). The analysis area is shown in Figure 1b.

	NWS	NS	GIZ	KAM	SAK	TER	NWS+NS	TOTAL
				Heat loss ($\times 10^{19}$ J)				
2003	10.53	3.37	2.26	2.69	1.91	0.86	13.91	21.62
2004	10.22	4.83	3.05	2.65	1.89	0.84	15.06	23.49
2005	9.27	5.30	2.87	2.92	0.88	0.96	14.56	22.19
Ave.	10.01	4.50	2.73	2.75	1.56	0.89	14.51	22.43
				Ice production ($\times 10^{11}$ m^3)				
2003	4.89	1.57	1.05	1.25	0.89	0.40	6.46	10.04
2004	4.75	2.25	1.42	1.23	0.88	0.39	6.99	10.91
2005	4.30	2.46	1.34	1.35	0.41	0.45	6.76	10.31
Ave.	4.65	2.09	1.27	1.28	0.72	0.41	6.74	10.42

Table 2. Similar to Table 1, except for average monthly values in the 3 winters.

	NWS	NS	GIZ	KAM	SAK	TER	NWS+NS	TOTAL
				Heat loss ($\times 10^{19}$ J)				
December	3.77	1.11	1.06	0.45	0.81	0.12	4.87	7.31
January	3.07	1.80	0.63	0.84	0.34	0.36	4.87	7.04
February	2.28	1.15	0.71	1.07	0.30	0.29	3.43	5.79
March	0.89	0.45	0.33	0.38	0.11	0.13	1.34	2.28
				Ice production ($\times 10^{11}$ m^3)				
December	1.75	0.51	0.49	0.21	0.38	0.05	2.26	3.40
January	1.43	0.83	0.29	0.39	0.16	0.17	2.26	3.27
February	1.06	0.53	0.33	0.50	0.14	0.13	1.59	2.69
March	0.41	0.21	0.15	0.18	0.05	0.06	0.62	1.06

Table 3. Sensitivities in heat loss to the atmosphere and cumulative ice production during winter (December–March) in the NWS polynya and major coastal polynyas (TOTAL) to perturbation in surface input. The sensitivity analysis is made by perturbing each variable positively and negatively. The re-estimated heat loss and cumulative ice production are averaged for 3 winters of 2002/2003–2004/2005 and are compared with the baseline calculation shown in Table 1.

	T2M	TD2M	U10M	CLO	HI
	Perturbation amplitude				
	1.2 (°C)	1.0 (°C)	14 (%)	16 (%)	0.05 (m)
	Change in heat loss/ice production (%)				
NWS	±5.9	±0.6	±5.5	±0.5	±30.9
TOTAL	±7.2	±1.2	±5.9	±0.5	±30.8

T2M, air temperature at 2 m; TD2M, dew point temperature at 2 m; U10M, wind speed at 10 m; CLO, cloud factor; HI, thin ice thickness.


0°
180°
60°N
30°N
0°
-30°C
-35°C
-20°C
0°C
-10°C
10°C
-10°C
20°C
(a)
140°E
150°E
160°E
60°N
55°N
50°N
45°N
Gizhiga Bay
GIZ
northern shelf
NS
NWS
northwest shelf
KAM
Kamchatka
Ayan
200
200
Sea of Okhotsk
SAK
Amur River
Sakhalin
Terpenia Bay
TER
200
3000
200
3000
3000
Hokkaido
Japan Sea
Pacific Ocean
(b)

Figure 1.

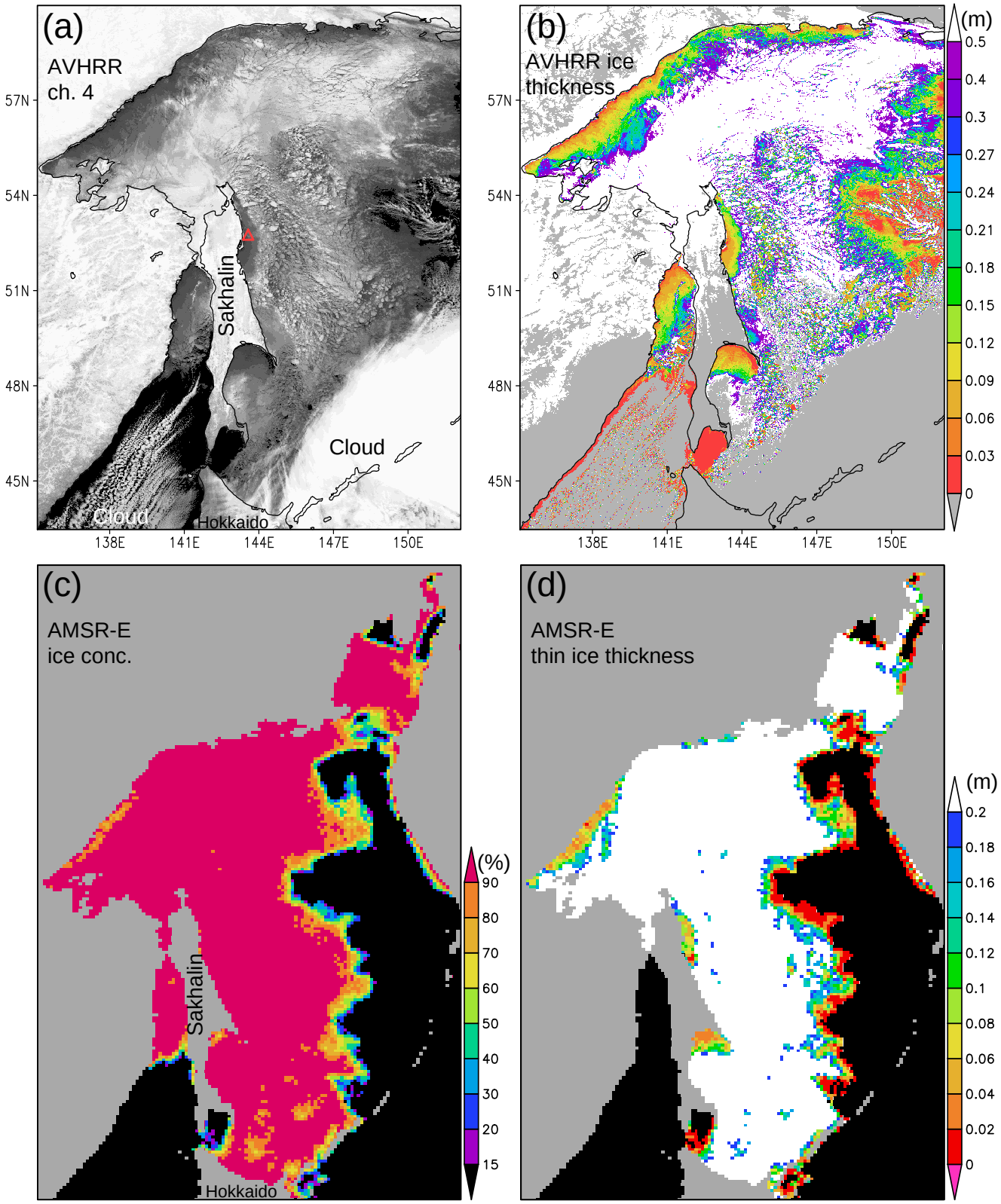
(a)
AVHRR
ch. 4
57N
54N
51N
48N
45N
138E
141E
144E
147E
150E
Sakhalin
Cloud
Cloud
Hokkaido
(b)
AVHRR ice
thickness
(m)
0.5
0.4
0.3
0.27
0.24
0.21
0.18
0.15
0.12
0.09
0.06
0.03
0
(c)
AMSR-E
ice conc.
Sakhalin
Hokkaido
(%)
90
80
70
60
50
40
30
20
15
(d)
AMSR-E
thin ice thickness
(m)
0.2
0.18
0.16
0.14
0.12
0.1
0.08
0.06
0.04
0.02
0

Figure 2.

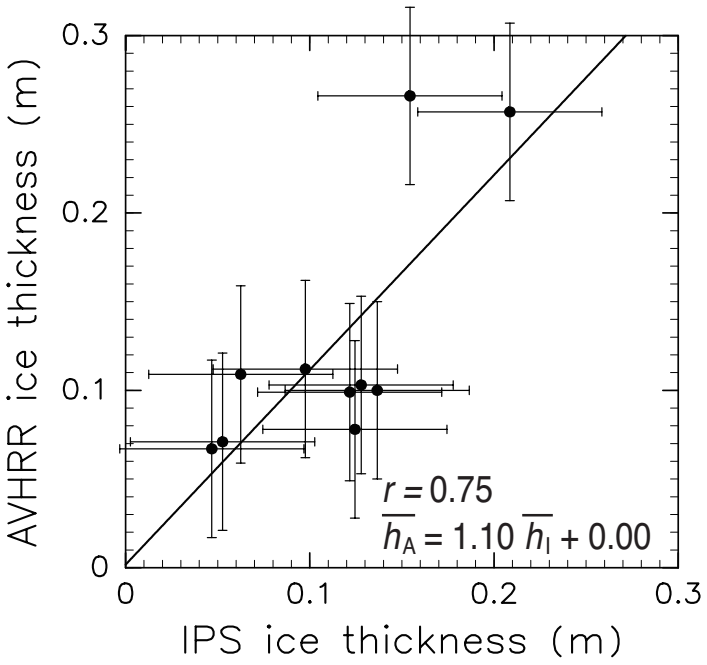
AVHRR ice thickness (m)
IPS ice thickness (m)
0
0.1
0.2
0.3
r = 0.75
$\overline{h_A} = 1.10\,\overline{h_I} + 0.00$

Figure 3.

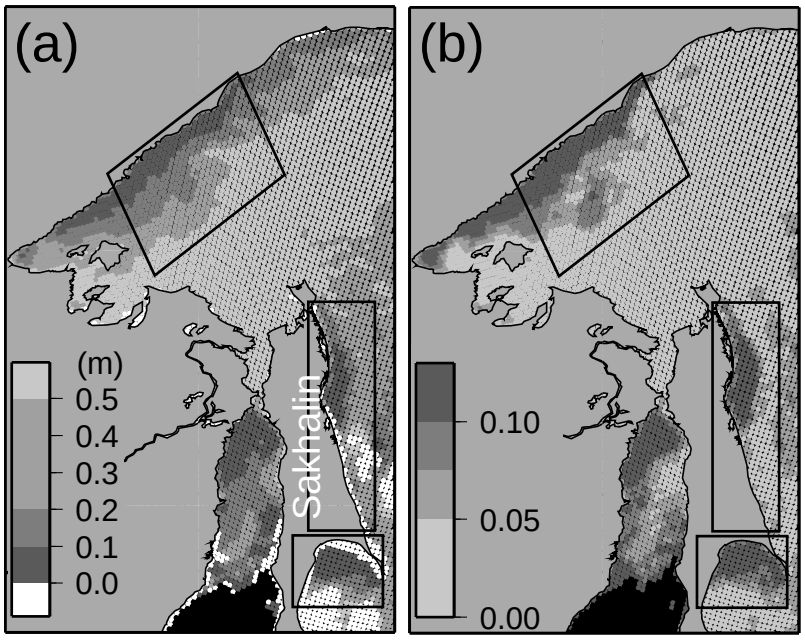

Figure 4.

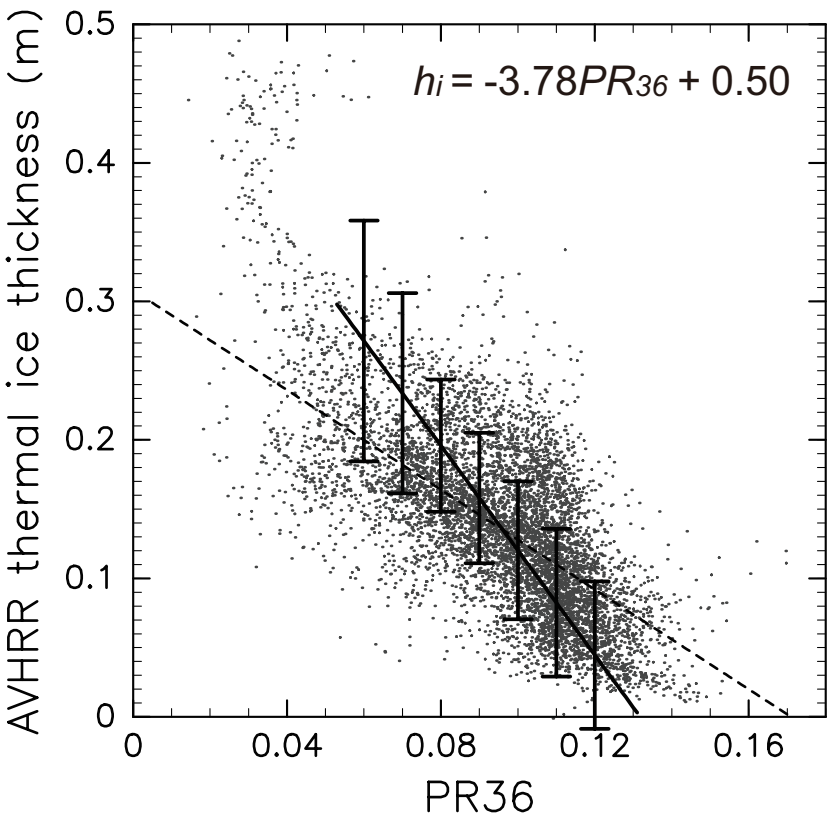
$h_i = -3.78PR_{36} + 0.50$
AVHRR thermal ice thickness (m)
0.5
0.4
0.3
0.2
0.1
0
0
0.04
0.08
0.12
0.16
PR36

Figure 5.

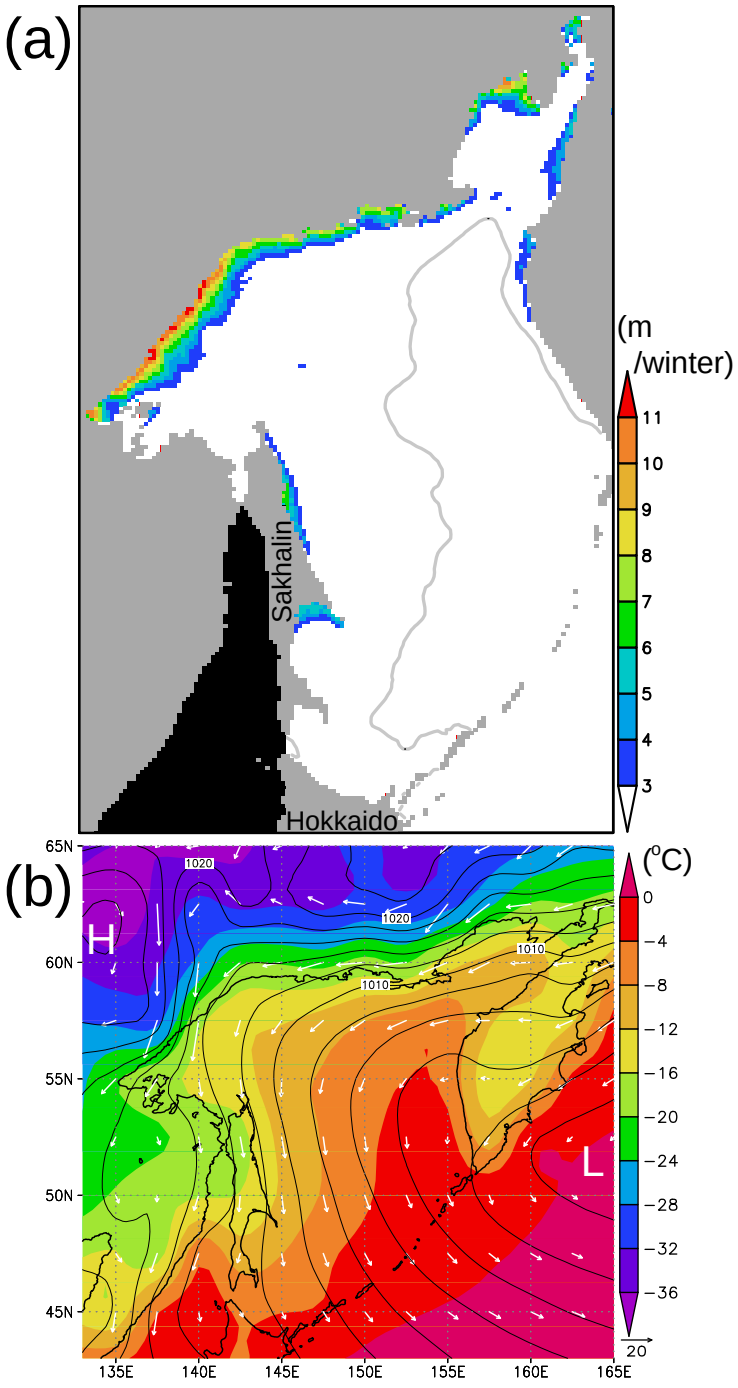
(a)
Sakhalin
Hokkaido
(m
/winter)
11
10
9
8
7
6
5
4
3
(b)
65N
60N
55N
50N
45N
135E
140E
145E
150E
155E
160E
165E
1020
1020
1010
1010
H
L
(°C)
0
−4
−8
−12
−16
−20
−24
−28
−32
−36
20

Figure 6.

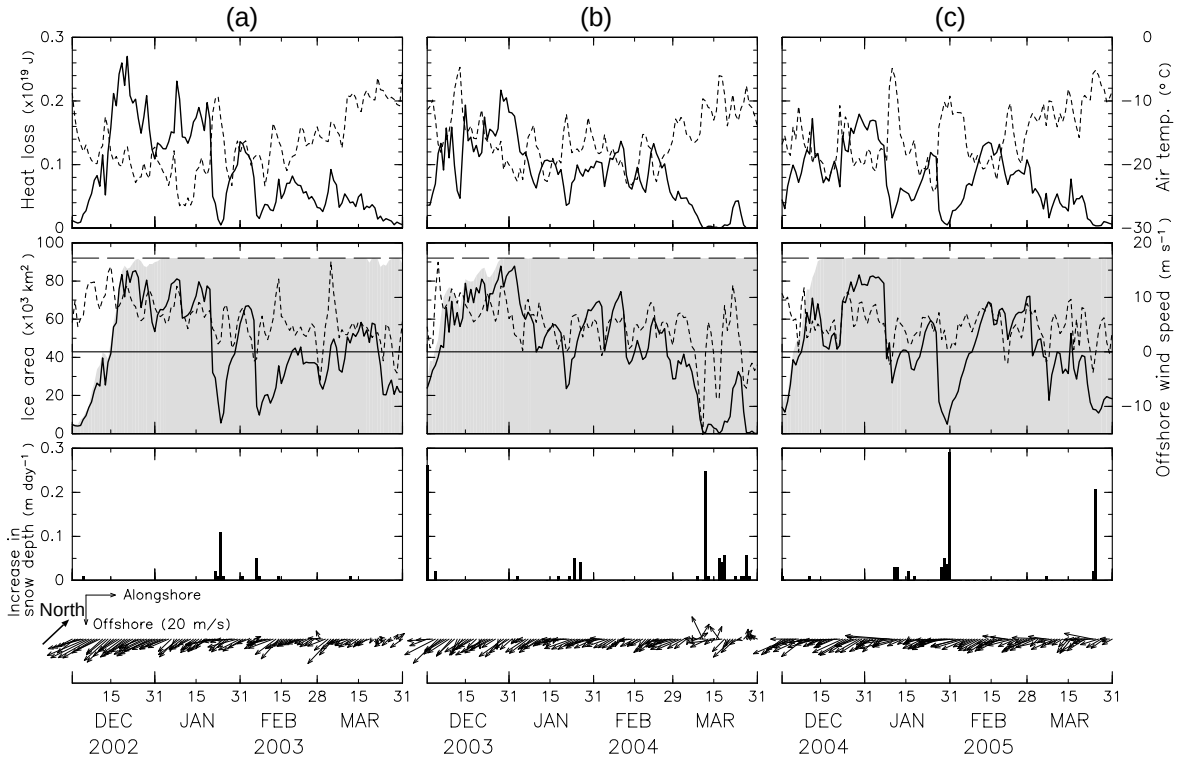
(a)
(b)
(c)
Heat loss (x10^19 J)
Air temp. (°C)
Ice area (x10^3 km^2)
Offshore wind speed (m s^-1)
Increase in snow depth (m day^-1)
North
Alongshore
Offshore (20 m/s)
15 31 15 31 15 28 15 31
DEC JAN FEB MAR
2002 2003
15 31 15 31 15 29 15 31
DEC JAN FEB MAR
2003 2004
15 31 15 31 15 28 15 31
DEC JAN FEB MAR
2004 2005

Figure 7.

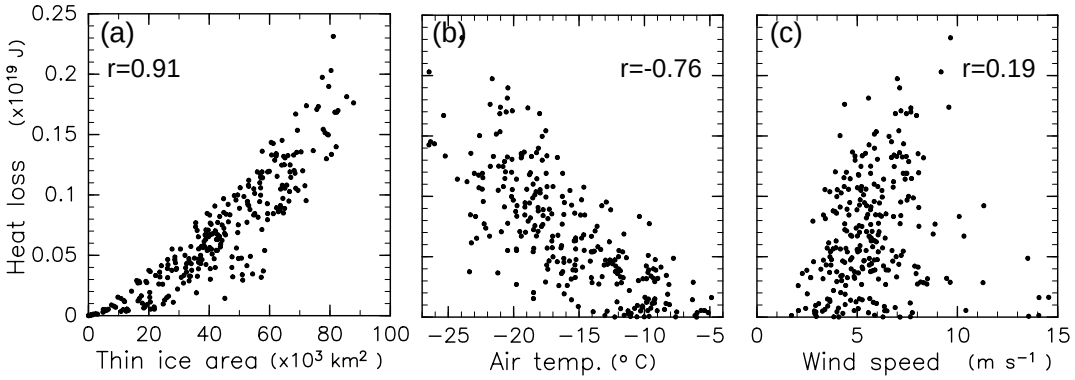
(a)
r=0.91
(b)
r=-0.76
(c)
r=0.19
Heat loss (x10^19 J)
0.25
0.2
0.15
0.1
0.05
0
0
20
40
60
80
100
Thin ice area (x10^3 km^2)
−25
−20
−15
−10
−5
Air temp. (° C)
0
5
10
15
Wind speed (m s^−1)

Figure 8.

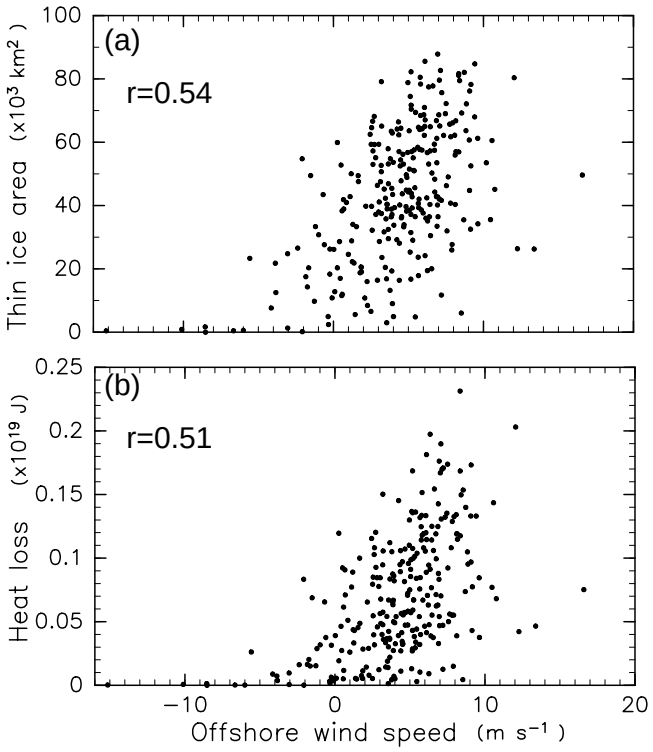
(a)
r=0.54
Thin ice area (x10³ km²)
100
80
60
40
20
0
(b)
r=0.51
Heat loss (x10¹⁹ J)
0.25
0.2
0.15
0.1
0.05
0
−10
0
10
20
Offshore wind speed (m s⁻¹)

Figure 9.

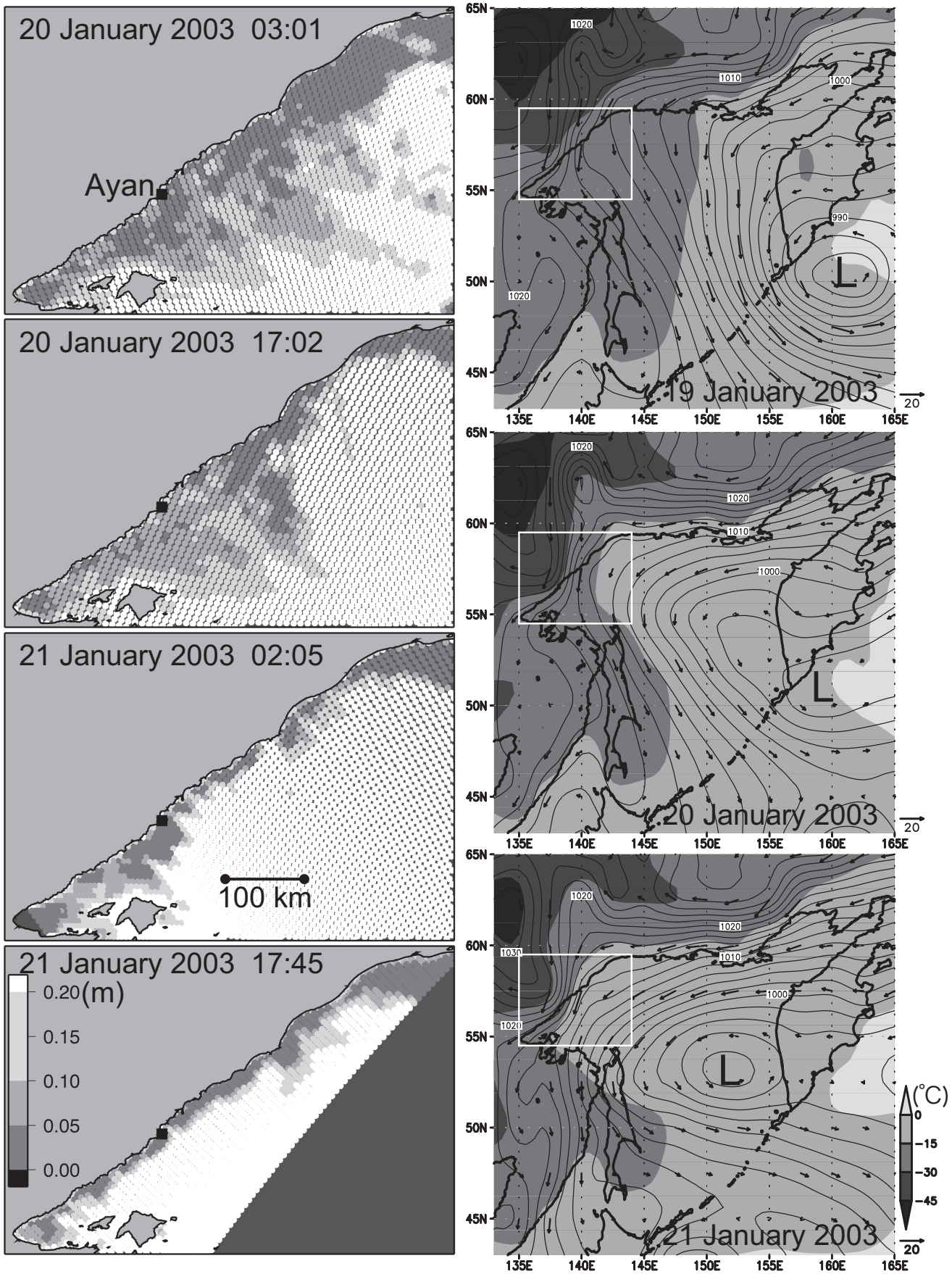
20 January 2003 03:01
Ayan
20 January 2003 17:02
21 January 2003 02:05
100 km
21 January 2003 17:45
0.20(m)
0.15
0.10
0.05
0.00
65N
60N
55N
50N
45N
135E
140E
145E
150E
155E
160E
165E
1020
1010
1000
990
L
19 January 2003
20 January 2003
21 January 2003
1030
(°C)
0
−15
−30
−45
20

Figure 10.